International Journal of Multiphase Flow 36 (2010) 460–466

Contents lists available at ScienceDirect

International Journal of Multiphase Flow

journal homepage: www.elsevier.com/locate/ijmulflow

Two-phase flow laden with spherical particles in a microcapillary

Young Won Kim [a,1], Jung Yul Yoo [a,b,*]

[a] Institute of Advanced Machinery and Design, Seoul National University, Seoul 151-744, Republic of Korea
[b] School of Mechanical and Aerospace Engineering, Seoul National University, Seoul 151-744, Republic of Korea

ARTICLE INFO

Article history:
Received 1 April 2009
Received in revised form 30 January 2010
Accepted 9 March 2010
Available online 15 March 2010

Keywords:
Solid–liquid two-phase flow
Lateral migration
Equilibrium position
Microcapillary

ABSTRACT

Solid–liquid two-phase flow in a finite Reynolds number range ($2 < Re < 12$), transporting neutrally-buoyant microspheres with diameters of 6, 10, and 16 μm through a 260-μm microcapillary, is investigated. A standard microparticle-tracking velocimetry (μ-PTV) that consists of a double-pulsed Nd:YAG laser, an epi-fluorescent microscope, and a cooled-CCD camera is used to examine the flow. The solid particles are visualized in view of their spatial distributions. We observe a strong radial migration of the particles across the flow streamlines at substantially small *Re*. The degree of particle migration is presented in terms of probability density function. Some applications based on this radial migration phenomena are discussed in conjunction with particle separation/concentration in microfluidic devices, where the spatial distribution of particles is of great importance. In doing so, we propose a particle-trajectory function to empirically construct the spatial distribution of solid particles, which is well correlated with our experimental data. It is believed that this function provides a simple method for estimating the spatial distribution of particles undergoing radial migration in solid–liquid two-phase flows.

1. Introduction

With an advance of miniaturization technology, transport of solid particles in microfluidic channels has drawn considerable attention from many areas of science and engineering, including flow cytometry (Kim and Yoo, 2009; Koch et al., 1999; Leshansky et al., 2007), chip-based miniaturized medical diagnostic kits (Minerick et al., 2002), detection of biological warfare agents (Cabrera and Yager, 2001), etc.

Conventionally, behaviors of solid particles in 'macro-scale flows' where channel length scales are typically on the order of centimeters (Segrè and Silberberg, 1962; Cox and Mason, 1971) have been widely investigated in conjunction with lateral migration. In the early days, Segrè and Silberberg (1961, 1962) observed that solid particles migrate to an equilibrium position at 0.6 times the radius of a tube having an inner diameter of 11.2 mm. Their work has influenced greatly the fluid mechanics studies regarding the migration and lift of dilute suspensions of neutrally buoyant spheres (Asmolov, 1999; Denson, 1965; Feng et al., 1994; Joseph and Ocando, 2002). The mechanism of this phenomenon was delineated by Ho and Leal (1974) who calculated the lateral force on a sphere using asymptotic theory in the Reynolds number range of $Re \ll 1$. Later, a broader range of *Re* has been considered in analyses (Schonberg and Hinch, 1989; Asmolov, 1999; Matas et al., 2009) and experiments (Matas et al., 2004).

On the other hand, only a limited number of papers on solid–liquid two-phase flows in microchannels have been reported in view of particle velocity (Staben and Davis, 2005; Xuan and Li, 2006), particle distribution (Staben and Davis, 2005), and lateral migration (Eloot et al., 2004; Kim and Yoo, 2008). Among those, the study on the lateral migration in microchannels has currently received much attention due to its wide prospective applications (Bhagat et al., 2008a,b; Carlo, 2009; Coupier et al., 2008; Kim and Yoo, 2008). Further, knowledge of spatial distributions of solid particles in circular-capillary-based microfluidic devices is of importance for the separation/concentration processes of biological particles, which directly utilize the radial migration phenomenon (Lin and Wickramasinghe, 2002; Poflee et al., 1994, 1998; Rakow and Fernald, 1991; Wickramasinghe et al., 2001). However, there is still lack of fundamental studies on the solid–liquid two-phase flows in the light of lateral migration in circular microchannels.

In this work we investigate solid–liquid two-phase flows in a circular cross-sectioned microchannel at finite *Re*'s. We carry out micro-particle-tracking experiments to determine the spatial distribution of solid particles undergoing radial migration. We also propose a particle-trajectory function to theoretically construct the spatial distribution of particles, which is correlated to the experimental data of this work.

* Corresponding author. Tel.: +82 2 880 7112; fax: +82 2 883 0179.
E-mail address: jyyoo@snu.ac.kr (J.Y. Yoo).
[1] Present address: BK21 School for Creative Engineering Design of Next Generation Mechanical and Aerospace Systems, Seoul National University, Seoul 151-744, Republic of Korea.

0301-9322/$ - see front matter © 2010 Elsevier Ltd. All rights reserved.
doi:10.1016/j.ijmultiphaseflow.2010.03.001

2. Experiment

2.1. Experimental method

Experimental method is explained in detail in an online Supplementary material. Briefly, as illustrated in Fig. 1, the experimental apparatus which is a standard μ-PTV/PIV system (Meinhart et al., 1999) consists of a double-pulsed Nd:YAG laser (SLI–PIV, Continuum Electro-Optics, USA), an inverted fluorescent microscope (IX50, Olympus, Japan), a cooled-CCD camera (SensiCam, PCO, Germany) and an air immersion objective with a numerical aperture $NA = 0.35$ (*magnification* $M = 10\times$, yielding that one pixel dimension is 1.28×1.28 μm). The experimental conditions are briefly summarized in Table 1. A teflon capillary with an inner diameter of $D_t = 260$ μm is adopted as the test channel. We used three sizes of fluorescent test particles with $D = 6 \pm 0.9$ μm, 10 ± 1.2 μm and 16 ± 2.2 μm (Duke Scientific, USA) to investigate the two-phase flow phenomena, while small tracer particles with $d = 2 \pm 0.2$ μm are mixed with respective test particles for measuring the background fluid velocity.

The volume fraction (= 0.1%) of the test particles *is maintained sufficiently low throughout* all the experiments so that particle–particle interactions can be neglected (Matas et al., 2004). The measurement is taken at a fixed location downstream of the capillary inlet, i.e., $L/D_t \approx 1620$, where $L = 42$ cm is the distance from the inlet. The ratios of capillary diameter to particle diameter are $D_t/D = 16.3$, 26 and 43.3 for the test particles with $D = 16$, 10 and 6 μm, respectively, in the range of $2 < Re < 12$. Further, the density matching between the fluid and the particles was achieved by using 22% glycerol–water mixture (Kim and Yoo, 2008).

2.2. Probability density function

To evaluate the radial migration of the test particles, a probability density function (*PDF*) has been adopted to present their spatial distribution along the radial direction, which is defined as follows:

$$f(r) = \frac{\sum_{q=1}^{q=700} N_q(r, r+dr)}{\sum_{r=0}^{r=R}\sum_{q=1}^{q=700} N_q(r, r+dr)}, \quad (1)$$

where $N_q(r,\ r+dr)$ is the number of particles between the radial positions r and $r+dr$ in the qth image frame at a given experimental condition, so that $\sum_{r=0}^{r=R}\sum_{q=1}^{q=700} N_q(r, r+dr)$ is the total number of particles summed over the radius R of the capillary and all the particle image frames. It is noted that $f(r)$ is a *PDF* representing the fraction of the number of particles between r and $r+dr$, such that $\int_0^R f(r)dr = 1$.

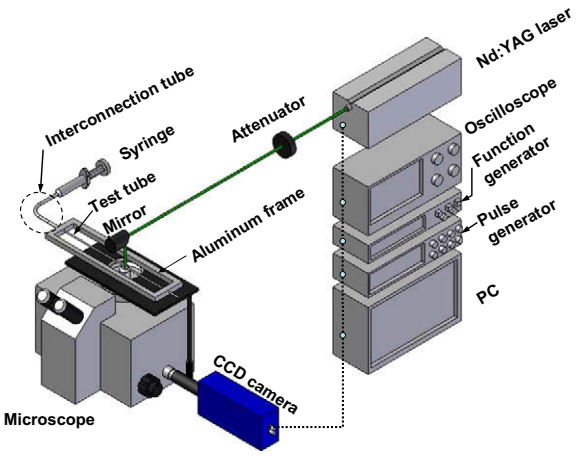

Fig. 1. Experimental setup of a standard micro-PTV system. A CCD camera and an Nd:YAG laser are triggered by a function generator and a pulse generator. The laser illuminates the test capillary via a mirror. Refractive index matching between the test capillary and the surrounding medium (water) was performed. An aluminum frame is used to keep the test capillary straight.

Table 1
Experimental conditions for the present study. The Reynolds number is based on the capillary diameter, the mean fluid velocity ($\overline{U}$) and the kinematic viscosity (v) of the fluid.

Parameters	
Capillary diameter (μm) (D_t)	260
Particle diameter (μm)	
Test particle diameter (D)	6, 10 and 16
Tracer particle diameter (d)	2
D_t/D	43.3, 26 and 16.3
Particle volume fraction (%)	
Test particle	0.1
Tracer particle	0.001
Reynolds number, $Re = \overline{U}D_t/v$	$2 < Re < 12$
Objective lens	
Magnification (M)	10×
Numerical aperture (NA)	0.35

2.3. Identification of test particles

Identification of test particles to achieve a depth-resolved measurement in PTV analysis is a very important consideration, in the sense that the in-focus particles should be exactly extracted from an image frame as data. Particle image intensity has been conventionally adopted as a criterion to identify particles in PTV/PIV measurements (Meinhart et al., 1999; Jin et al., 2004). However, when identifying relatively large solid particles in microchannel flows, the method based on the 'mean image-intensity gradient' (hereafter denoted as β), which represents how well-defined the boundary of a particle image is, provides a better depth-wise resolution for such purposes (Kim and Yoo, 2008). The intensity gradient at a given pixel element can be calculated through a first-order difference scheme in terms of pixel elements along the radial direction. Then β is obtained by taking the mean of the image intensity gradient. The previous work of the authors of the present study is referred to for more details of this calculation procedure (Kim and Yoo, 2008).

Thus, to determine the measurement depth (optical-slice thickness), we obtained β for each test particle ($D = 10$ and 16 μm) by taking images of the particle at discrete axial positions. A PZT linear stage (PUML40, Piezo Technology, Korea) with submicron resolution was used to axially move the focal plane of an objective lens. The calibration curves of the mean image intensity-gradient are shown in Fig. 2 in terms of β^*, obtained from normalizing β by its maximum value. The measurement depths are approximately 14 and 20 μm for test particles with $D = 10$ and 16 μm, respectively, when $\beta^* = 0.8$ is taken for each curve. They correspond to 5.3% and 7.7% of the internal diameter of the test capillary ($D_t = 260$ μm) for $D = 10$ and 16 μm, respectively, which gives a very good depth-wise resolution. As for $D = 6$ μm, which is much small compared to the channel diameter, the image intensity itself was adopted to identify in-focus particles or particles with well-defined outlines by applying a reasonable intensity threshold value, which is conventionally practiced in μ-PTV/PIV experiments (Meinhart et al., 1999).

3. Experimental results and discussion

The location of a test particle is determined by applying a 2D Gaussian curve fit to the particle intensity distribution, which is

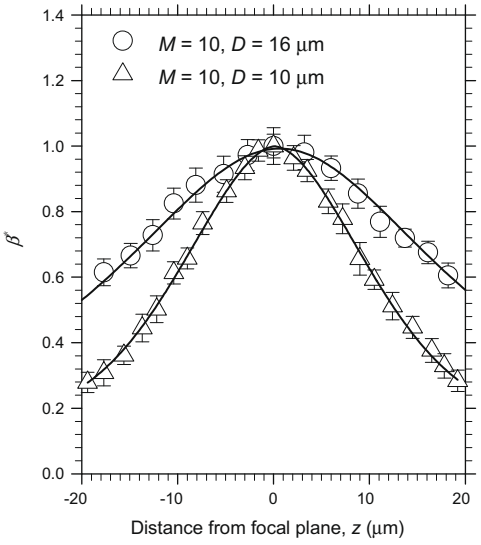

Fig. 2. Calibration curves that determine the measurement depths of the present imaging technique for $D = 10$ and 16 μm with $M = 10\times$, which is presented in terms of β^*, obtained from normalizing β by its maximum value. The value of β^* represents how well-defined the boundary of a particle image is. Thus, it has a maximum value near the focal plane at $z = 0$.

the same method as used for the tracer particle. The error in determining the center of a test particle is about ±1 pixel. The number of radial bins employed for analyzing the spatial distribution of test particles is 30, so that the width of a radial bin is 4.33 μm.

3.1. Observation of radial migration

Fig. 3 shows the distributions of 16-μm test particles transported through the capillary, which reveals the evolution of the particle distribution as *Re* increases. On the abscissa, '0.0' and '1.0' denote the centerline and the wall of the capillary, respectively. At $Re = 2.93$, a weak migration is observed. However, as *Re* further increases, the particles accumulate at an equilibrium position of $r/R \approx 0.63$ due to strong radial migration phenomenon, so that a distinctive peak of *PDF* is observed as well as a region devoid of particles near the center. Smaller particles ($D = 6$ and 10 μm) exhibit relatively inactive radial migrations, compared to the largest particles ($D = 16$ μm) at a given *Re*, which is not provided here for brevity. In any event, particle equilibrium positions are estimated to be at $r_e/R \approx 0.63$ and 0.69 for $D = 10$ and 6 μm, respectively. This strong radial migration of test particles was also observed at a relatively larger $Re \approx 60$ in square cross-section microchannel flows (Kim and Yoo, 2008). There is a similarity of migration trend between circular and rectangular channels in the sense of the "tubular-pinch" effect being formed. Besides, earlier experimental results (Segrè and Silberberg, 1962; Matas et al., 2004) on the particle distributions in large size channels would not be significantly different from that in a microchannel, except that the degree of particle migration is easily controllable in a microchannel by utilizing the channel scale effect, which is discussed in the following.

First, spatial distribution of particles is compared to those of the previous works for comparable values of migration parameters, as shown in Fig. 4. The 'hit' number of the original work of Segrè and Silberberg (1962), which represents the particle distribution, is converted to a *PDF* for the convenience of comparison. The numbers of radial bins are 30, 25 and 12, respectively for the present study, Matas et al. (2004) and Segrè and Silberberg (1962). It is noted that a maximum value of *PDF* (PDF_m) is influenced by the number of bins. Therefore, a direct comparison of the data of

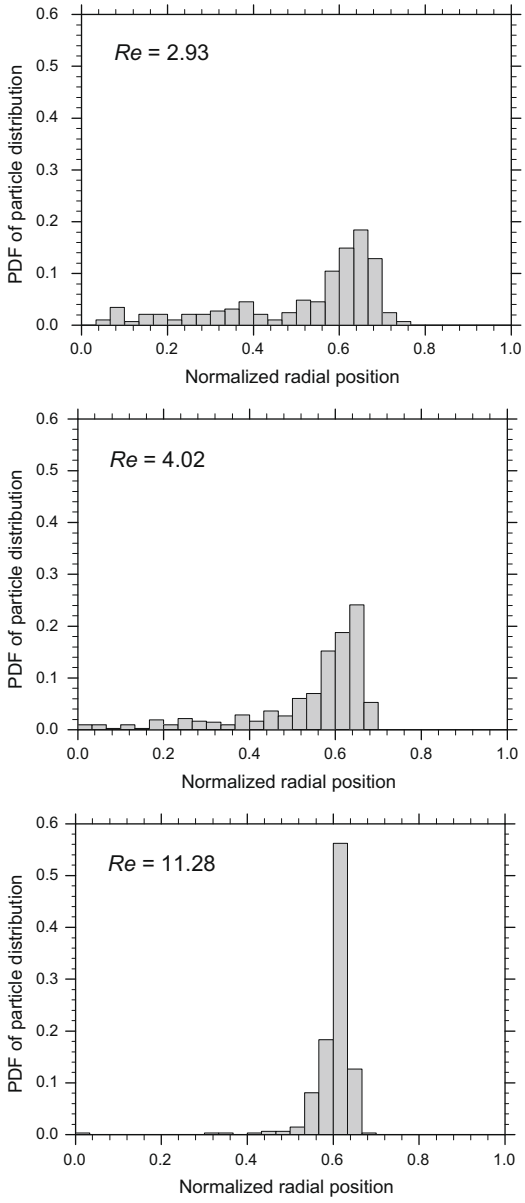

Fig. 3. *PDF*'s representing the spatial distributions of test particles over the radial position at different Reynolds numbers ($L/D_t \approx 1620$ and $D_t/D = 16.3$). An accumulation of the particles at the equilibrium position of $r/R \approx 0.63$ is prominently observed with increasing *Re*.

Fig. 4 may not be so meaningful due to the uneven numbers of bins.

However, Fig. 4 provides qualitatively the characteristics of the particle distribution in view of a local-accumulation phenomenon, which enables to assess whether particle migration is fully developed or not. The data of Segrè and Silberberg (1962) are much dispersed radially when compared to the present data, which is possibly due to the fact that their observation is made at a nearer measurement station of $L/D_t \approx 100$. In contrast, the data of the present study and Matas et al. (2004), commonly indicate apparent occurrence of particle migration with almost no particles near the channel centerline. Nonetheless, there are large discrepancies in *Re* between the two results. We are able to observe fully-developed particle migration at much smaller *Re* by inducing a large value of $L/D_t \approx 1620$ resorting to the channel scale effect, where $L \approx 43$ cm. In fact, a realization of a fully-developed particle migration with a narrow spatial distribution as shown in Fig. 4 from the

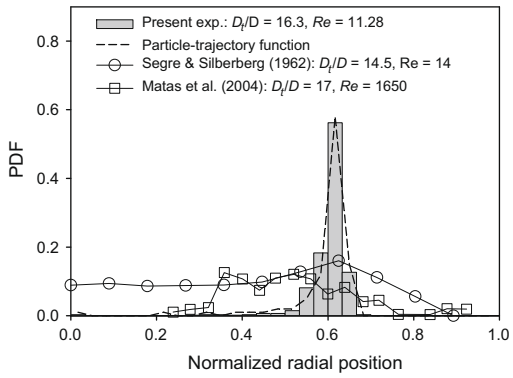

Fig. 4. Comparison of the particle distribution obtained from the present experiment with those of the previous works for comparable values of migration parameters. The 'hit' number of the original work of Segrè and Silberberg (1962), which represents the particle distribution, is converted into a *PDF* for the convenience of comparison. The numbers of radial bins are 30, 25 and 12, respectively for the present study, Matas et al. (2004) and Segrè and Silberberg (1962). Particle-trajectory function is to be defined later in Section 4.1.

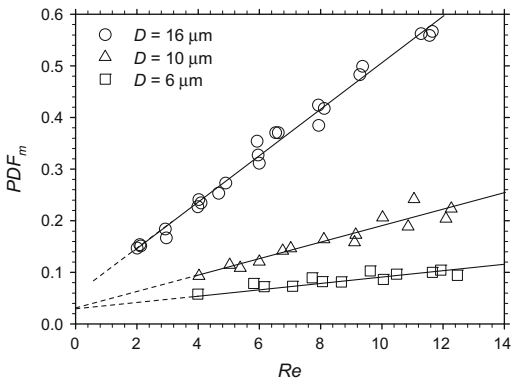

Fig. 5. PDF_m vs. *Re* for each particle size. Solid lines are linear curve fits. The dashed lines extrapolated are converged to $PDF_m \approx 0.03$ at $Re = 0$ for two smaller particle sizes, which is in very good agreement with the case when particles are uniformly distributed, e.g., at $Re = 0$.

present experimental data is very important to microfluidic applications (Bhagat et al., 2008a,b).

It is also noted that Matas et al. (2004) increased *Re* up to 1650 at $L/D_t = 310$ (where $L = 2.5$ m), because a critical *Re* for fully-developed particle migration is estimated to be 1500 at their measurement station of $L/D_t = 310$. The particles are more broadly distributed over the channel cross-section compared to the present data. This broad distribution might be due to the oscillations of the particle trajectories at high *Re* (e.g., $Re > 550$), which are damped out at small *Re* (Denson, 1965). Interestingly, the particle equilibrium position shifts to the wall with increasing *Re*, which was demonstrated also by Matas et al. (2004) at $Re > 60$ for various ratios between channel and particle sizes. However, we have not observed any major changes in the equilibrium position with increasing *Re* up to the present upper limit ($Re \approx 12$) at a given particle size. This is because the critical *Re* at which the equilibrium position starts to increase is estimated to be in the range of $20 < Re < 30$ (Schonberg and Hinch, 1989). Up to now, there is no experimental result showing the particle equilibrium position as *Re* further increases, including the critical *Re* in a circular Poiseuille flow, which is being examined as our future work.

3.2. Maximum PDF

Maximum *PDF* (PDF_m) is defined as a *PDF* value at the peak position of the particle distribution, which provides a criterion of whether the particle migration is fully developed or not. For instance, the particles may be still in the transient region at lower values of $Re = 2.93$ and 4.02. However, it is shown that the particles are almost absent near the center of the capillary at $Re = 11.28$ in Fig. 3. In other words, the majority of the solid particles have migrated to the equilibrium position of $r_e/R \approx 0.63$, so that they are in the fully-developed particle migration region. We therefore judge arbitrarily that particle migration is nearly fully developed when $PDF_m \approx 0.5$. Linear curve fits are made to correlate PDF_m as a function of *Re* for each test particle size in Fig. 5. The correlations as for the smaller particles of $D = 6$ and 10 μm indicate that radial migrations of these particles are still in the transient region (i.e., $PDF_m < 0.5$ for $4 < Re < 12$). On the other hand, when the particle distribution is exactly uniform such as in the case of $Re = 0$, a *PDF* or PDF_m value is about 0.033 (which is calculated as $PDF = \int_0^R f(r)dr/N = 1/30 \approx 0.033$), where *N* is the number of the radial bins used to construct *PDF*'s. Interestingly, this is in very good agreement with the extrapolations of the linear curve fits for the test particles with $D = 6$ and 10 μm. However, the extrapolation of the linear curve fit for $D = 16$ μm at $Re < 2$ is deviated from this value.

It is noteworthy that PDF_m as a function of *Re* in Fig. 5 can provide an empirical correlation for the "particle-trajectory function" which will be discussed in Section 4. More importantly, PDF_m and the particle equilibrium position, which can be identified by analyzing the spatial distribution of particles, are crucial for some applications that will be discussed in the following section.

3.3. Applications

There have been numerous attempts to separate and concentrate micro beads and biological particles in circular-capillary-based microfluidic devices that directly take advantage of the radial migration phenomena (Lin and Wickramasinghe, 2002; Poflee et al., 1994, 1998; Rakow and Fernald, 1991; Wickramasinghe et al., 2001). Here, controlling the particle equilibrium position as well as particle distributions are essential to the efficiency of the system performance. In-depth discussions of the radial migration in terms of its applications are given in an Electronic Annex.

4. Particle-trajectory function (*PTF*)

4.1. Derivation of particle-trajectory function

In the light of the importance of estimating the spatial distribution of particles that undergo radial migration, we propose a particle-trajectory function as a tool for predicting the spatial disposition of these particles. Derivation of this function depends upon the trend curve of the particle trajectory under lateral migration. Good examples of these curves were provided elsewhere (Ho and Leal, 1974; Feng et al., 1994; Segrè and Silberberg, 1962). The characteristics of this curve can be summarized as follows: the trajectory of a particle undergoing radial migration draws an exponentially increasing curve in the downstream direction when it is released in the inner region, i.e., $r < r_e$, while it draws an exponentially decreasing curve when released in the outer region, i.e., $r > r_e$. Thus, we assume that a mathematical expression for the trajectory of a particle in the inner region can be written as follows:

$$\frac{dr}{dx} \approx kr \text{ for } r < r_e, \tag{2}$$

while that in the outer region can be expressed as

$$\frac{dr}{dx} < 0 \quad \text{for } r > r_e, \tag{3}$$

where k is a proportional constant. Next, near the equilibrium position, the following expression should hold:

$$\frac{dr}{dx} \to 0 \quad \text{as } r \to r_e. \tag{4}$$

We obtain a generalized formula by combining Eqs. (2–4) as follows:

$$\frac{dr}{dx} = kr\left(1 - \frac{r}{r_e}\right). \tag{5}$$

Solution of Eq. (5) can be obtained by using a method of separation of variables and partial fraction expansion, which is given as follows:

$$r^*(x^*) = \frac{r_0^* \exp(k^* x^*)}{1 - r_0^*/r_e^* + r_0^*/r_e^* \exp(k^* x^*)}, \tag{6}$$

where all variables are normalized, such that $r^* = r/R$, $r_0^* = r_0/R$, $r_e^* = r_e/R$, $x^* = x/D_t$ and $k^* = kD_t$: r_0 is the initial radial position of a particle and x is the axial distance from the capillary inlet. Figs. 6 and 7 respectively show sample simulation results (particle trajectories (top) and the corresponding *PDF*'s (bottom)) for $k^* = 0.0007$ and $k^* = 0.002137$, which exhibit high dependence on the value of k^*. In the simulation, we take $r_e^* = 0.63$ based on our experimental observation for $D_t/D = 16.3$. The initial positions of the particles at $L/D_t = 0$ are uniformly spaced along the normalized radial distance. Then, a set of 50 particles are released from $L/D_t = 0$ and traced until they reach $L/D_t = 1620$. *PDF*'s are constructed with all the traced particle locations at $L/D_t \approx 1620$. Next, we explain how to determine the values of k^* for the *PDF*'s obtained from the particle-trajectory functions

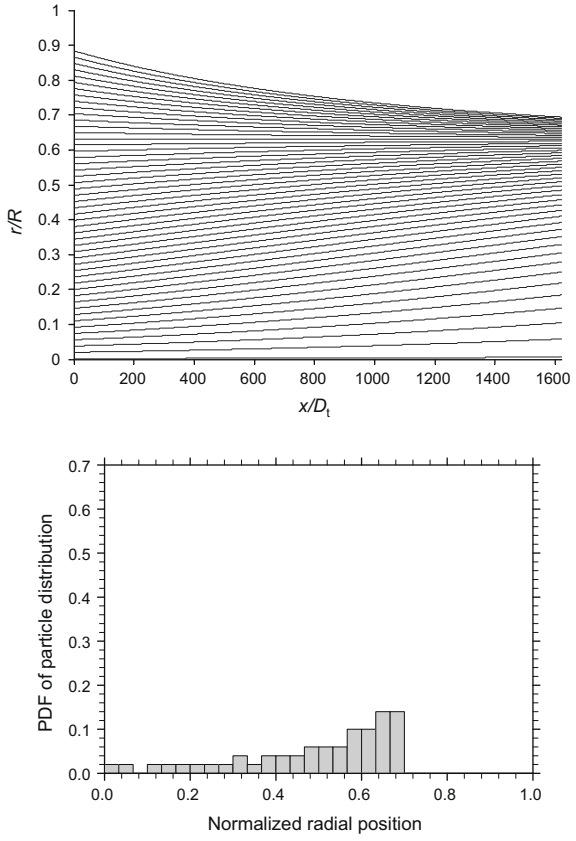

Fig. 6. Simulation results of the particle-trajectory function for $k^* = 0.0007$ (top: particle trajectories, bottom: corresponding particle distribution). Fifty particles are released from $L/D_t = 0$ and traced until they reach $L/D_t \approx 1620$. The *PDF* is constructed from the radial positions of the traced particles at $L/D_t \approx 1620$.

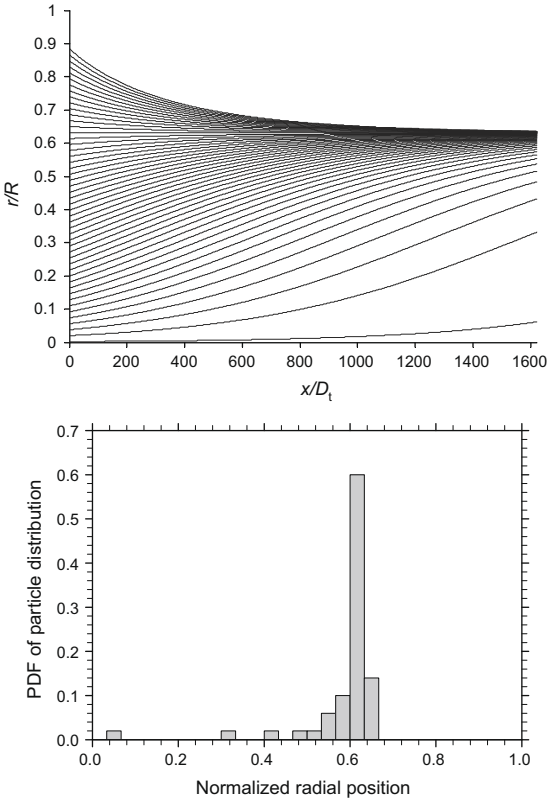

Fig. 7. Simulation results of the particle-trajectory function for $k^* = 0.002137$ (top: particle trajectories, bottom: corresponding particle distribution). Fifty particles are released from $L/D_t = 0$ and traced until they reach $L/D_t \approx 1620$. The *PDF* is constructed from the radial positions of the traced particles at $L/D_t \approx 1620$.

to best match with our experimental data and discuss the related implications of k^* in the following subsection.

4.2. Empirical correlations

Basically, we determine k^* through a trial-and-error procedure in such a manner that the constructed *PDF* from Eq. (6) best describes the experimental data for fixed values of D and Re. This procedure consists of the following two steps.

(i) We consider a set of the spatial distribution of particles obtained from the experiment (e.g., Fig. 3a for $D = 16$ μm at $Re = 2.93$).
(ii) We find an optimum k^* through a trial-and-error procedure such that the simulated *PDF* from Eq. (6) best matches with the experimental data, where 50 particles are used for the construction of the *PDF*.

The simulated *PDF*'s for respective particle sizes at a fixed $Re \approx 8$, are shown in Fig. 8, which is in good agreement with the experimental data. *PDF*'s based on the theory proposed by Tachibana (1973) are also compared with the present experimental data. The particle equilibrium position estimated by the constructed *PDF* according to the theory (Tachibana, 1973) is likely to be shifted toward the wall as the particle size decreases. This is because the theory underestimates the present experimental data, which is more prominent when the particle size becomes smaller. However, absolute values of the *PDF*'s for both studies are in very good agreement in the case of the largest particle size.

Next, recall from Fig. 5 that PDF_m represents the level of particle migration (i.e., the higher the PDF_m is, the more prominent the par-

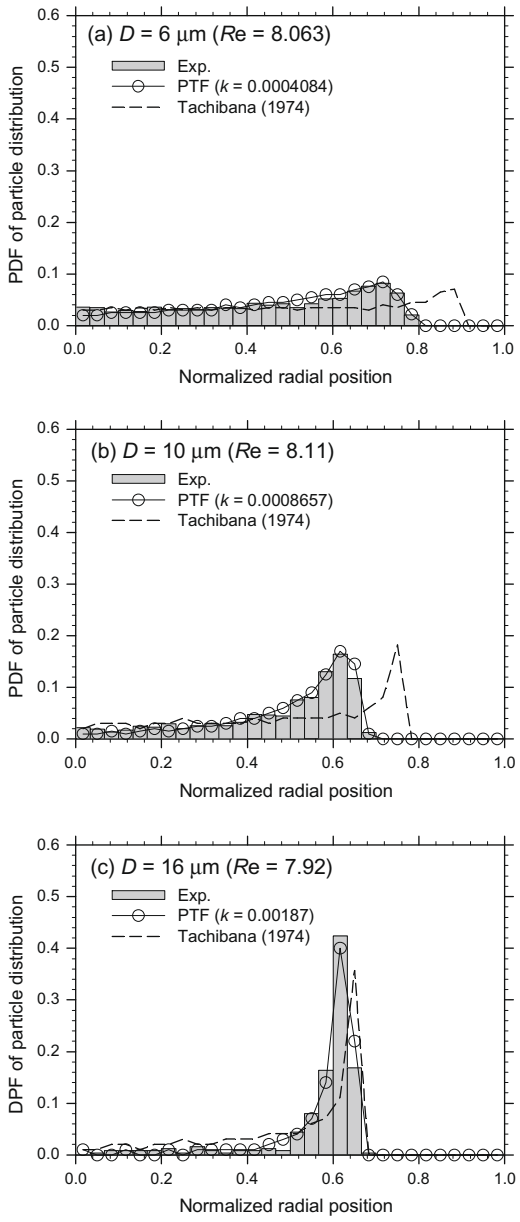

Fig. 8. Comparison of *PDF*'s among the present experiment, the present PTF, and the theory proposed by Tachibana (1973) at a fixed $Re \approx 8$.

ticle migration is). Similarly, the level of the particle migration can be also controlled by k^*, as illustrated in Figs. 6 and 7. These facts enable to express the relation of k^* vs. PDF_m as $k^* \propto f(PDF_m)$ or $k^* = PDF_m^{\alpha}$. Based on the linear curve fits of Fig. 5, k^*'s for respective particle sizes are given as follows:

$$k_1^* = (0.0062Re + 0.0333)^{\alpha_1} \quad \text{for } D = 6\ \mu m, \tag{7}$$

$$k_2^* = (0.0162Re + 0.0333)^{\alpha_2} \quad \text{for } D = 10\ \mu m, \tag{8}$$

$$k_3^* = (0.0452Re + 0.0528)^{\alpha_3} \quad \text{for } D = 16\ \mu m, \tag{9}$$

where α_1, α_2, and α_3 are the exponents to be determined empirically. However, it is noted in passing that the above relations can not naturally give $k = 0$ at $Re = 0$ because they are originally based on the assumption that the particle migration occurs no matter how slight it is (i.e., $Re > 0$).

Trend of k^* vs. Re for each test particle is shown in Fig. 9, by which the *PDF*'s from the particle-trajectory function are well correlated with the experimental data. Linear curve fittings are performed for two small particle sizes, while a 3rd order curve fitting is made for $D = 16$ μm. Thus, the exponents for the test particles of 6, 10 and 16 μm are given as follows:

$$\alpha_1 = 0.062Re + 2.6, \tag{10}$$

$$\alpha_2 = 0.170Re + 2.6, \tag{11}$$

$$\alpha_3 = 0.0054Re^3 - 0.0593Re^2 + 0.702Re + 2.5. \tag{12}$$

We further find the correlation between k^* and the standard deviation σ of the particle distribution as shown in Fig. 10, because the standard deviations are important characteristics for microfluidic applications. Interestingly, σ increases linearly against k^* regardless of the particle size. In the shaded region, particle migration is expected to be fully developed.

5. Further discussion

Theoretical studies for calculating the trajectory of a particle undergoing lateral migration have utilized both the perturbation method (Asmolov, 1999; Ho and Leal, 1974; Schonberg and Hinch, 1989) and DNS (Feng et al., 1994; Joseph and Ocando, 2002; Zhu, 2000). The perturbation method is usually based on the assumption that a particle size is very small compared to the channel gap, and a particle is not too close to the wall. Although these restrictions do not apply to DNS, it does require much computational time and high computational cost. Furthermore, in many cases, both methods calculate the particle trajectory on a single particle level. However, many particles should be traced to construct their spatial distributions in the statistical sense (Cho et al., 2005). Although a number of particles are also traced in this

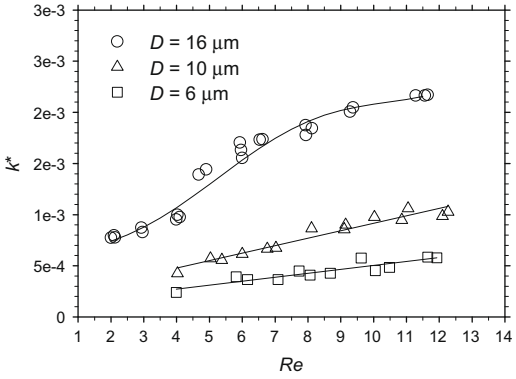

Fig. 9. Parameter k^* vs. Re, for each test particle, at which the particle-trajectory function best predicts the experimental data. Solid lines are the curve fits.

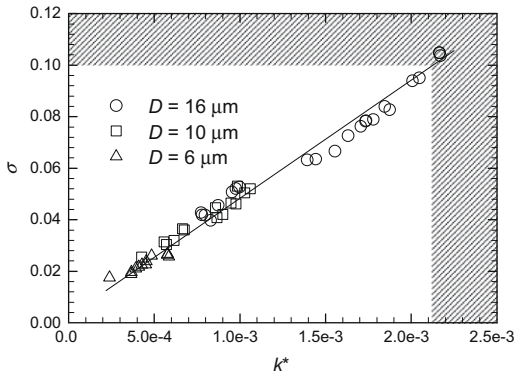

Fig. 10. Standard deviation σ of the particle distribution as a function of k^*. The solid line serves to guide the eyes. In the shaded region, particle migration is expected to be fully developed.

work to obtain a single *PDF*, the present calculation utilizing *PTF* is fairly simple.

In practice, spatial distributions of solid particles under radial migration is mainly affected by the particle size relative to the tube diameter, Reynolds number and measurement location from the inlet (L/D_t). We have proposed the particle-trajectory function for the limited cases of $L/D_t \approx 1620$, and $Re < 12$. However, it is expected to further generalize this function by considering such parameters in broader ranges through a more systematic and extensive study.

6. Conclusions

Solid–liquid two-phase flow in a microcapillary was investigated by using a μ-PTV system. The spatial distributions of solid particles under a radial migration in a circular microchannel at small Re ($2 < Re < 12$) were demonstrated. It is shown that the solid particles undergo strong radial migration with increasing Re, which gather at certain equilibrium position. Besides, a fully developed particle migration was observed at much smaller Re, compared to the previous experimental work on macro scale flows. A PDF_m obtained in terms of Re provides an estimation of the degree of particle migration. A particle-trajectory function is proposed to empirically represent the particle distribution, which is well correlated with the experimental data of the present work. Understanding the spatial distributions of solid particles is essential to the separation/concentration processes in microfluidic devices, which directly employ the principle of the radial migration phenomenon. A more systematic observation considering a broader range of the ratio between particle and capillary diameters, and the Reynolds numbers is needed for better understanding and utilization of this phenomenon.

Acknowledgement

This work was supported by the Korea Research Foundation Grant funded by the Korean Government (MOEHRD) (KRF-0420-20070058).

Appendix A. Supplementary material

Supplementary data associated with this article can be found, in the online version, at doi:10.1016/j.ijmultiphaseflow.2010.03.001.

References

Asmolov, E.S., 1999. The inertial lift on a spherical particle in a plane Poiseuille flow at large channel Reynolds number. J. Fluid Mech. 381, 63–87.

Bhagat, A.A.S., Kuntaegowdanahalli, S.S., Papautsky, I., 2008a. Enhanced particle filtration in straight microchannels using shear-modulated inertial migration. Phys. Fluids 20, 101702.

Bhagat, A.A.S., Kuntaegowdanahalli, S.S., Papautsky, I., 2008b. Inertial microfluidics for continuous particle filtration and extraction. Microfluid. Nanofluid. (doi: 10.1007/s10404-008-0377-2).

Cabrera, C.R., Yager, P., 2001. Continuous concentration of bacteria in a microfluidic flow cell using electrokinetic techniques. Electrophoresis 22, 355–362.

Carlo, D.D., 2009. Inertial microfluidics. Lab Chip 9, 3038–3046.

Cho, S.H., Choi, H.G., Yoo, J.Y., 2005. Direct numerical simulation of fluid flow laden with many particles. Int. J. Multiphase Flow 31, 435–451.

Coupier, G., Kaoui, B., Podgorski, T., Misbah, C., 2008. Noninertial lateral migration of vesicles in bounded Poiseuille flow. Phys. Fluids 20, 111702.

Cox, R.G., Mason, S.G., 1971. Suspended particles in fluid flow through tubes. Annu. Rev. Fluid Mech. 3, 291–316.

Denson, C.D., 1965. Particle Migration in Shear Fields. Ph.D. Dissertation, University of Utah.

Eloot, S., Bisschop, F.D., Verdonck, P., 2004. Experimental evaluation of the migration of spherical particles in three-dimensional Poiseuille flow. Phys. Fluids 16, 2282–2293.

Feng, J., Hu, H.H., Joseph, D.D., 1994. Direct simulation of initial value problems for the motion of solid bodies in a Newtonian fluid. Part 2. Couette and Poiseuille flows. J. Fluid Mech. 277, 271–301.

Ho, B.P., Leal, L.G., 1974. Inertial migration of rigid spheres in two-dimensional unidirectional flows. J. Fluid Mech. 65, 365–400.

Jin, S., Huang, P., Park, J., Yoo, J.Y., Breuer, K.S., 2004. Near-surface velocimetry using evanescent wave illumination. Exp. Fluids 37, 825–833.

Joseph, D.D., Ocando, D., 2002. Slip velocity and lift. J. Fluid Mech. 454, 263–286.

Kim, Y.W., Yoo, J.Y., 2008. The lateral migration of neutrally-buoyant spheres transported through square microchannels. J. Micromech. Microeng. 18, 065015.

Kim, Y.W., Yoo, J.Y., 2009. Axisymmetric flow focusing of particles in a single microchannel. Lab Chip 9, 1043–1045.

Koch, M., Evans, A.G.R., Brunnschweiler, A., 1999. Design and fabrication of a micromachined coulter counter. J. Micromech. Microeng. 9, 159–161.

Leshansky, A.M., Bransky, A., Korin, N., Dinnar, U., 2007. Tunable nonlinear viscoelastic "Focusing" in a microfluidic device. Phys. Rev. Lett. 98, 234501.

Lin, W.C., Wickramasinghe, S.R., 2002. Leukocyte fractionation by lateral migration. Trans. IChemE. 80, 83–87.

Matas, J.-P., Morris, J.F., Gauzzelli, É., 2004. Inertial migration of rigid spherical particles in Poiseuille flow. J. Fluid Mech. 515, 171–195.

Matas, J.-P., Morris, J.F., Gauzzelli, É., 2009. Lateral force on a rigid sphere in large-inertia laminar pipe flow. J. Fluid Mech. 621, 59–67.

Meinhart, C.D., Wereley, S.T., Santiago, J.G., 1999. PIV measurements of a microchannel flow. Exp. Fluids 27, 414–419.

Minerick, A.R., Ostafin, A.E., Chang, H.-C., 2002. Electrokinetic transport of red blood cells in microcapillaries. Electrophoresis 23, 2165–2173.

Poflee, N.M., Rakow, A.L., Werntz, M., Pons, M.N., 1994. Stagewise design for concentration of Spirulina platensis based on lateral migration with flow through vertical tees. Bioseparation 4, 237–246.

Poflee, N.M., Rakow, A.L., Ryan, K., Dahl, S., Dandy, D.S., 1998. Maximization of recovery of spirulina platensis in a staged process based on inertial migration. Sep. Sci. Technol. 33, 915–931.

Rakow, A.L., Fernald, D., 1991. Concentration of *spirulina* suspensions by radial migration with flow through vertical tees. Biotechnol. Prog. 7, 343–347.

Schonberg, J.A., Hinch, E.J., 1989. Inertial migration of a sphere in Poiseuille flow. J. Fluid Mech. 203, 517–524.

Segrè, G., Silberberg, A., 1961. Radial particle displacements in Poiseuille flow of suspensions. Nature 189, 209–210.

Segrè, G., Silberberg, A., 1962. Behaviour of macroscopic rigid spheres in Poiseuille flow. Part 2. Experimental results and interpretation. J. Fluid Mech. 14, 136–157.

Staben, M.E., Davis, R.H., 2005. Particle transport in Poiseuille flow in narrow channels. Int. J. Multiphase Flow 31, 529–547.

Tachibana, 1973. On the behaviour of a sphere in the laminar tube flows. Rheol. Acta. 12, 58–69.

Wickramasinghe, S.R., Lin, W.-C., Dandy, D.S., 2001. Separation of different sized particles by inertial migration. Biotechnol. Lett. 23, 1417–1422.

Xuan, X., Li, D., 2006. Particle motions in low-Reynolds number pressure-driven flows through converging-diverging microchannels. J. Micromech. Microeng. 16, 62–69.

Zhu, M., 2000. Direct Numerical Simulation of Solid–Liquid Flow of Newtonian and Viscoelastic Fluids. Ph.D. Dissertation, University of Pennsylvania.